



# Global existence of solutions to a tear film model with locally elevated evaporation rates

Yuan Gao<sup>a</sup>, Hangjie Ji<sup>b,\*</sup>, Jian-Guo Liu<sup>b,c</sup>, Thomas P. Witelski<sup>b</sup>

<sup>a</sup> School of Mathematical Sciences, Fudan University, PR China

<sup>b</sup> Department of Mathematics, Duke University, United States

<sup>c</sup> Department of Physics, Duke University, United States

## HIGHLIGHTS

- A coupled system of non-conservative PDEs for a tear film model is analyzed.
- Heterogeneous evaporation drives dynamics in film thickness and osmolarity.
- The regularity of global solutions to the model for a certain parameter range is obtained.
- Locally elevated evaporation rates can yield interesting finite-time rupture–shock phenomenon.
- Convergence to equilibrium solutions and infinite-time thinning are investigated numerically.

## ARTICLE INFO

### Article history:

Received 3 January 2017

Received in revised form

10 March 2017

Accepted 13 March 2017

Available online 21 March 2017

Communicated by S. Wang

### Keywords:

Tear film

Rupture

Thin film equation

Evaporation

Osmolarity

Finite-time singularity

## ABSTRACT

Motivated by a model proposed by Peng et al. (2014) for break-up of tear films on human eyes, we study the dynamics of a generalized thin film model. The governing equations form a fourth-order coupled system of nonlinear parabolic PDEs for the film thickness and salt concentration subject to non-conservative effects representing evaporation. We analytically prove the global existence of solutions to this model with mobility exponents in several different ranges and present numerical simulations that are in agreement with the analytic results. We also numerically capture other interesting dynamics of the model, including finite-time rupture–shock phenomenon due to the instabilities caused by locally elevated evaporation rates, convergence to equilibrium and infinite-time thinning.

© 2017 Elsevier B.V. All rights reserved.

## 1. Introduction

In this article, we study the regularity of solutions to a one-dimensional nonlinear partial differential equation system for a fluid film height  $h(x, t)$  and salt concentration (also called the osmolarity)  $s(x, t)$  on a finite domain,  $0 \leq x \leq L$ ,

$$h_t = -(h^n h_{xxx})_x - h^m (\bar{S} - s), \quad (1.1a)$$

$$s_t = s_{xx} + \left( \frac{h_x}{h} - h^{n-1} h_{xxx} \right) s_x + s(\bar{S} - s) h^{m-1}. \quad (1.1b)$$

This family of PDEs is motivated by a non-conservative lubrication model for evaporating tear films on human eyes. Based on the

model proposed by Peng et al. [1], a spatial variation in a thin lipid layer on the tear film leads to locally elevated evaporation rates of the tear film, which in turn affects the local salt concentration in the liquid film. In our model (1.1) the influences of the lipid layer thickness on osmolarity are included in the effective salt capacity function,  $\bar{S}(x) \in L^\infty([0, L])$ . This will be taken to be a given positive function with increased values over some portion of the domain, corresponding to elevated evaporation rates (and decreased lipid concentrations). Starting from initial data  $(h_0(x), s_0(x))$  at time  $t = 0$  which satisfy  $h_0 > 0$  and  $0 < s_0 \leq \|\bar{S}\|_\infty$ , the dynamics will be subject to no-flux and normal-contact boundary conditions

$$\begin{aligned} h_x(0) = h_x(L) = 0, \quad h_{xxx}(0) = h_{xxx}(L) = 0, \\ s_x(0) = s_x(L) = 0. \end{aligned} \quad (1.1c)$$

\* Corresponding author.

E-mail address: [hangjie@math.duke.edu](mailto:hangjie@math.duke.edu) (H. Ji).

The mobility exponents  $n$  and  $m$  in (1.1) are introduced to analyze and separate the influences of the conservative and non-conservative fluxes in the model respectively. The term  $(h^n h_{xxx})_x$  in the model is due to capillary forces, the terms  $h^m(\bar{S} - s)$  and  $s(\bar{S} - s)h^{m-1}$  are related to evaporative effects,  $s_{xx}$  corresponds to the diffusion of the salt concentration, and the term  $(h^{-1}h_x - h^{n-1}h_{xxx})s_x$  is related to the convective transport of the salt. Details of the formulation from the physical model will be discussed further in Section 2. The original model in [1] corresponds to (1.1) with the exponent values  $m = 0$  and  $n = 3$ .

The total mass of salt,  $\mathcal{S}$ , in the liquid film is of fundamental interest, and one can obtain the conservation of this quantity by multiplying (1.1a) by  $s$ , multiplying (1.1b) by  $h$  and then integrating the sum of the two equations,

$$\mathcal{S}(t) = \int_0^L hs \, dx, \quad \mathcal{S}(t) = \mathcal{S}(0) = \int_0^L h_0 s_0 \, dx. \quad (1.2)$$

We will use the conservation of  $\mathcal{S}$  in the proof of the boundedness of  $h$  and the study of equilibrium solutions of the system. The total mass of the liquid film in the system is not conserved and its rate of change can be obtained from integrating (1.1a) and applying the boundary conditions,

$$\mathcal{M}(t) = \int_0^L h \, dx, \quad \frac{d\mathcal{M}}{dt} = - \int_0^L h^m(\bar{S} - s) \, dx. \quad (1.3)$$

We note that with initial data  $0 < s_0 < \|\bar{S}\|_\infty$  and  $h_0 > 0$ , the osmolarity is always bounded by  $\|\bar{S}\|_\infty$ . This result will be shown formally in the proof of Theorem 1 in Section 3 by the weak maximum principle in [2, Lemma 7.6]. Namely,  $s(x, t)$  is not guaranteed to be bounded by  $\bar{S}(x)$  pointwise; consequently it is not clear if  $\mathcal{M}(t)$  is necessarily decreasing in time.

The imposed osmolar capacity  $\bar{S}(x)$  is essential in determining the dynamics of the model (1.1). Although in previous models [1], it was assumed that  $\bar{S}$  is smooth and takes the form of a Gaussian distribution, the regularity of solutions to (1.1) is not sensitive to the smoothness of  $\bar{S}$ . For instance, with  $\bar{S}$  given by a positive indicator function,

$$\bar{S}(x) = \begin{cases} 100 & \text{for } 0.5 < x < 1.5, \\ 2 & \text{otherwise,} \end{cases} \quad (1.4)$$

a typical evolution of  $h$  and  $s$  over the domain  $0 \leq x \leq 2$  with  $(m, n) = (3.5, 4.5)$  is presented in Fig. 1, with figures (a) and (b) showing the dynamics of height and salt concentration profiles in (1.1) and figures (c) and (d) illustrating the evolution of some key properties for those profiles. Spatially uniform initial conditions for both film thickness and salt concentration are used, corresponding to states produced by opened eyes after a blink [3]. Starting from normalized initial conditions  $h_0 = s_0 = 1$ , the film thickness  $h$  decreases with an increasing spatial variation driven by the locally elevated  $\bar{S}$ , while the osmolarity rises due to the evaporation and is elevated more quickly near the center of the domain. Later, the symmetry of the film is broken and  $h$  reaches its minimum at  $x \approx 0.8$  and  $x \approx 1.2$ . This is difficult to see in plot (a), but is depicted in the plot (c) where  $h_{\min}(t) = \min_x h(x, t)$  is no longer attained at the center of the domain. The localized elevation in osmolarity  $s$  is a transient effect with  $h_{\min}(t)$  approaching zero algebraically and  $s$  evolving slowly as  $t \rightarrow \infty$ .

The mobility exponents,  $m$  and  $n$ , are crucial in determining the qualitative behavior of the PDE model. In Section 2 we will review the motivating tear film model which corresponds to (1.1) with exponents  $(m, n) = (0, 3)$ . The modified tear film Eqs. (1.1) are then proposed. In Section 3, the global and local existence of solutions to (1.1) in several different ranges of  $(m, n)$  are proved analytically. These regularity results, together with other interesting dynamics of the model, are then further investigated with numerical simulations in Section 4.

## 2. A physical model for tear film break-up driven by evaporation

Human eyes are coated with a thin precorneal tear film which is a bio-fluid with a complex composition but can be approximated in terms of a viscous fluid with dissolved salt and a lipid layer. Tear film thinning and break-up during interblink periods are observable clinically and play a key role in dry eye disorders. While many mechanisms have been proposed in the literature [4–6], it is now generally agreed that evaporation is one of the most important factors for the tear film break-up phenomenon [7]. In addition to evaporation effects, capillarity and osmolarity also contribute to the dynamics of the tear film. In particular, experiments have shown that the local increase of osmolarity is evident along with the reduced tear film thickness as the break-up occurs. For a thorough discussion on the dynamics of tear film, we refer readers to [3].

Since the average aqueous tear film thickness (approximately  $10^{-6}$  m) [8] is much thinner than the average radius of curvature of the eye (about  $10^{-2}$  m), we follow the literature [3,9] to assume that the substrate underneath the tear film is flat. In addition, it is appropriate to use the lubrication approximation to model the evolution of the tear film, since the exposed surface of the eye (called the palpebral fissure) is about  $10^3$  times larger than the average tear film thickness, and the tear film can be modeled as a viscous flow at a low Reynolds number. The dynamics of thin viscous film flows have been studied extensively for the past decade due to their fundamental importance in coating flows, painting, biological applications like tear films [3], and other applications in science and engineering. There is a large literature on the numerical and modeling studies of evaporating thin films [10], and some of the results can be applied to the study of tear films. For the characterization of thin film flows with surfactant [11,12], a suspension of heavy particles [13], or drying paint layers [14,15], an additional PDE for surfactant concentration or particle concentration is usually incorporated into the PDE system.

The conservation of water leads to the dimensionless governing equation for the film thickness  $h$ ,

$$\frac{\partial h}{\partial t} = - \frac{\partial}{\partial x} (uh) - J_e + J_w, \quad (2.1)$$

with the flow velocity  $u$  given by [1]

$$u = -h^2 \frac{\partial p}{\partial x}, \quad (2.2)$$

where the dynamical pressure  $p$  is given by the combination of the generalized conjoining pressure  $\Pi(h)$  and the linearized curvature  $h_{xx}$ ,

$$p = \Pi(h) - h_{xx}, \quad (2.3)$$

and  $t$  and  $x$  are temporal and spatial variables. Here we take the conjoining pressure to be  $\Pi(h) = -\epsilon/h^3$  with the rescaled Hamaker constant  $\epsilon > 0$  which represents the wetting property of the corneal surface. The two non-conservative contributions  $J_e$  and  $J_w$  correspond to the evaporative flux and osmotic weeping flux and will be described below in detail.

The dynamics of the salt concentration is governed by a second dimensionless evolution equation which describes the local conservation of salt in terms of diffusion and convective transport of the aqueous film,

$$\frac{\partial}{\partial t} (hs) = \frac{\partial}{\partial x} \left( h \frac{\partial s}{\partial x} - ush \right). \quad (2.4)$$

This form guarantees that the total salt mass is conserved

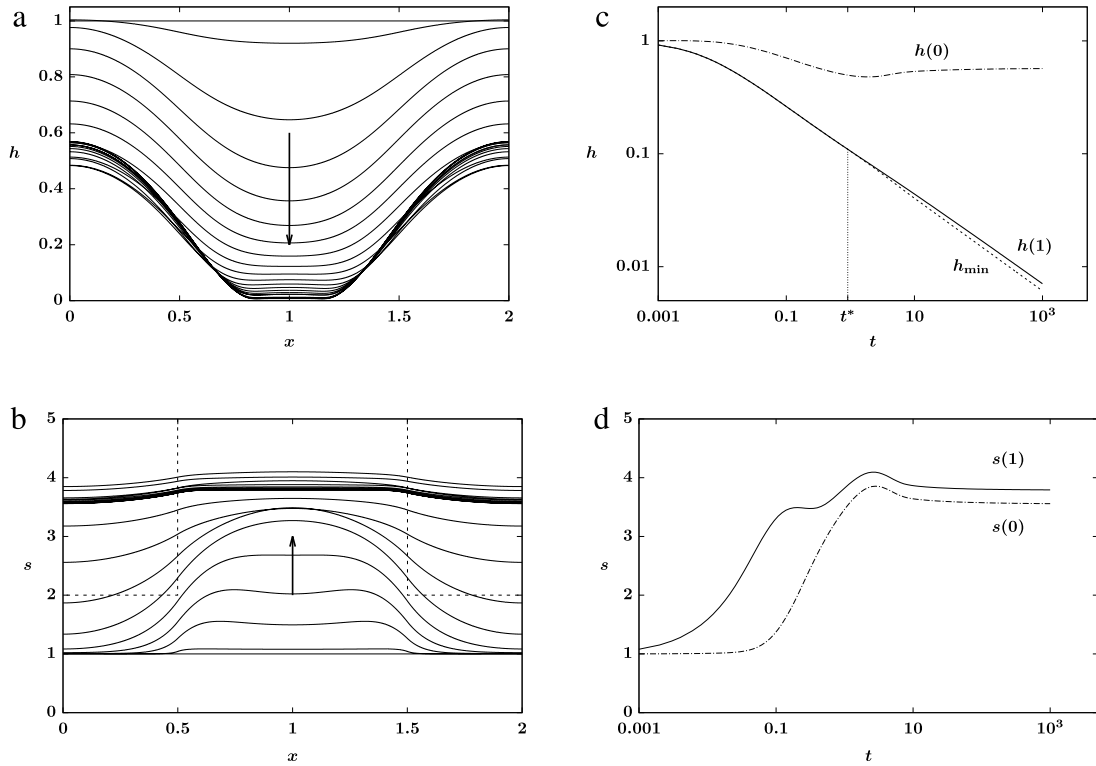


**Fig. 1.** Numerical solution of (1.1) with  $(m, n) = (3.5, 4.5)$  starting from constant initial data  $h_0 = s_0 = 1$  for  $0 \leq x \leq 2$  driven by non-conservative flux with  $\bar{S}(x)$  given by (1.4): (a) and (b) are solution profiles for  $h$  and  $s$ , where the capacity  $\bar{S}$  is plotted in dashed line; (c) and (d) present the evolution of the  $h$ ,  $s$  solutions at the edge ( $x = 0$ ) and center ( $x = 1$ ) of the domain, respectively. The minimum film thickness  $h_{\min}(t)$  monotonically decreases and approaches 0 as  $t \rightarrow \infty$ , while the osmolarity  $s$  is locally elevated in the early stage and the spatial variations decay in the later stage. Starting from a critical time  $t^* \approx 0.9$ , the minimum of  $h$  is attained at two points away from the center ( $x = 1$ ) of the domain.

$$\int hs \, dx = \int h_0 s_0 \, dx. \quad (2.5)$$

The osmotic weeping flux,  $J_w$ , is assumed to be proportional to the difference between the salt concentration in the tear film and a reference osmolarity constant,  $S_0$ ,

$$J_w = s - S_0. \quad (2.6)$$

Several different mathematical models have been studied [16–19] for the mechanisms of the tear film break-up driven by evaporation, and the major differences among these models are in the physical interpretation of the evaporation effects involved in the tear film. For instance, Braun [3] derived the form of evaporative mass flux

$$J_e = \frac{E(1 + \delta p)}{\bar{K} + h}, \quad (2.7)$$

where  $\bar{K} > 0$  measures the thermal resistances to mass transfer at the fluid–vapor interface,  $E > 0$  characterizes the ratio of viscous timescale to the non-conservative timescale, and  $\delta$  is a nondimensional parameter for evaporation. This type of evaporative flux was first proposed by Burelbach et al. [20] in a one-sided evaporating thin film model where the dynamics of the fluid is assumed decoupled from the evolution of the vapor, and was later investigated by Ajaev [21,22] for a more detailed evaporation model. Later a revised version of (2.7) was further studied in [16]. More recently the influence of surfactant was also included in the evaporative mass flux in [17].

In 2014, Peng et al. [1] derived a tear film break-up model with instabilities driven by evaporation effects by treating the lipid layer on the fluid tear film as a barrier to local evaporation from the underlying tear film. Assuming that the evolution of the lipid layer is

static compared to the dynamics of the aqueous film, they imposed a fixed spatially varying profile to approximate the local variations in the lipid concentration. Since reduced amounts of the lipid cause locally elevated liquid evaporation rates relative to that of the film in surrounding regions [23,18], they included an additional mass-transfer resistance term to account for the counteraction due to the lipid concentration. The resulting evaporative mass flux  $J_e$  is then obtained by solving a coupled system for  $J_e(x, t)$  and the temperature of the liquid–vapor interface. In order to simplify the evaporative flux term, we consider the same influence of lipid layer as an obstruction to evaporation but ignore the latent heat of water vaporization, and write the evaporative flux as

$$J_e = \frac{P_s e^{\delta p} - P_\infty}{R_L(x) + R_G} \sim \frac{E}{R_L(x) + R_G} \quad \text{for } \delta \rightarrow 0 \text{ with } E = P_s - P_\infty, \quad (2.8)$$

where  $R_L(x)$  measures the mass-transfer resistance through the tear film lipid layer which depends on the lipid concentration,  $R_G$  represents the mass-transfer resistance in ambient air,  $P_s$  and  $P_\infty$  are nondimensional saturation vapor pressure at cornea and in the environment, respectively. This form of evaporative flux is comparable to (2.7) when the contribution from the dynamical pressure  $p$  to the evaporation is negligible,  $h \ll \bar{K}$ , and water evaporation from the tear film is obstructed by both resistances through the spatially dependent lipid layer and through the air phase. Consequently, using (2.6) and (2.8), the total non-conservative flux from evaporative and osmolarity weeping flows can be written conveniently in terms of an  $\bar{S}(x)$  function as

$$-J_e + J_w = s - \left( \frac{E}{R_L(x) + R_G} + S_0 \right) = s - \bar{S}(x). \quad (2.9)$$

To summarize, from (2.1) and (2.4) the nondimensional governing equations for the evolution of tear film thickness  $h$  and the osmolarity  $s$  in human eyes can be represented by

$$h_t = - \left[ h^3 \left( h_{xx} + \frac{\epsilon}{h^3} \right) \right]_x - (\bar{S} - s), \quad (2.10a)$$

$$s_t = s_{xx} + \left( \frac{h_x}{h} - h^2 \left( h_{xx} + \frac{\epsilon}{h^3} \right) \right) s_x + \frac{s}{h} (\bar{S} - s), \quad (2.10b)$$

with the associated boundary conditions (1.1c), where (2.10b) is obtained from applying the product rule to the time derivative term and substituting Eq. (2.10a) into Eq. (2.4).

It is interesting to note that both the fourth-order term due to surface tension and the second-order term due to conjoining pressure in (2.10a) are stabilizing. Since our major interest is to examine the mechanism of possible breakdowns of the tear film model (2.10), in this work we neglect the conjoining pressure by setting  $\epsilon = 0$  in (2.10) and focus on the competition between the fourth-order regularizing term and the non-conservative contributions. To get a better understanding of the PDEs, we consider the generalized model (1.1) to explore the key features of tear-film break-up with power-law mobility functions for both conservative and non-conservative contributions. In particular, in order to regularize the non-conservative effects in the PDEs, modified versions of the non-conservative terms are considered with the original terms  $(\bar{S} - s)$  in Eqs. (2.10) multiplied by a regularizing factor  $h^m$ . It is worth noting that the physical model (2.10) for tear films with  $\epsilon = 0$  corresponds to the case  $(m, n) = (0, 3)$  of the generalized PDE system (1.1).

In the present work, the PDE system (1.1) is investigated from the perspective of both analytical and numerical studies. Specifically, it will be shown numerically in Section 4 that the tear film model (2.10) exhibits a novel finite-time rupture-shock phenomenon, that is, at a critical point  $x = x_c$ , the film thickness  $h(x_c, t) \rightarrow 0$ , along with  $|s_x(x_c)| \rightarrow \infty$  as a critical time  $t_c$  is approached. The finite-time singularity phenomenon admitted in this model inspires us to investigate the modified PDE system (1.1) in other parameter ranges.

### 3. Regularity of solutions to the generalized model (1.1)

In this section, we study the regularity of solutions to (1.1) with appropriate initial data and show that the existence of strong solutions depends on different ranges of the exponents  $m$  and  $n$ . Specifically, by proving the existence of upper and lower bounds for the film thickness and the salt concentration, we show that under certain circumstances both the film thickness and the salt concentration are prevented from reaching zero or blowing-up. The main result for global strong solutions to Eqs. (1.1) with the exponents  $(m, n)$  that satisfy  $n = m + 1$ ,  $3 \leq m < 4$ , and the local existence of strong solutions to (1.1) with  $m, n \geq 0$  are stated in the following two theorems. The proof of the global existence is then presented, and a sketch of the proof of the local existence result is included in Remark 2.

**Theorem 1 (Global Existence).** Suppose that  $n = m + 1$ ,  $3 \leq m < 4$ ,  $\bar{S}(x) \in L^\infty([0, L])$ , and for any integer  $k \geq 2$ , the initial data  $h_0(x) \in H^k([0, L])$ ,  $s_0(x) \in H^{k-2}([0, L])$  satisfy  $0 < \eta \leq h_0(x)$ ,  $0 < \lambda \leq s_0(x) \leq \|\bar{S}(x)\|_\infty$  for some positive constants  $\eta, \lambda > 0$ . Then for any  $T > 0$ , there exist unique solutions  $h(x, t) \in L^\infty([0, T]; H^k([0, L])) \cap L^2([0, T]; H^{k+2}([0, L]))$  and  $s(x, t) \in L^\infty([0, T]; H^{k-2}([0, L])) \cap L^2([0, T]; H^{k-1}([0, L]))$  that satisfy (1.1ab) with the initial data  $h_0, s_0$  and the boundary conditions (1.1c). Moreover,  $s(x, t)$  satisfies

$$0 < \lambda \leq s(x, t) \leq \|\bar{S}\|_\infty \quad \text{for all } t \in [0, T], \quad (3.1)$$

and there exist positive bounds  $h_m(T)$ ,  $H_m(T)$  such that

$$0 < h_m(T) \leq h(x, t) \leq H_m(T) \quad \text{for all } t \in [0, T], \quad (3.2)$$

where  $h_m(T)$ ,  $H_m(T)$  depend on  $\eta, \lambda, \|h_0 s_0\|_1, \|h_0\|_1, \|\bar{S}\|_\infty$  and  $T$ .  $\diamond$

We define  $\eta = \min_x h_0(x)$  and  $\lambda = \min_x s_0(x)$ . The uniform lower and upper bound estimates in (3.2) are crucial for the higher order estimates, which guarantee the existence of the global solutions. We will use some basic estimates and two apriori assumptions to obtain the uniform lower and upper bound estimates in (3.2) and then verify those apriori assumptions. Specifically, we will show that the condition  $m < 4$  comes from the upper bound  $H_m(T)$  and that the condition  $3 \leq m$  comes from the lower bound  $h_m(T)$ . Then standard compactness arguments can be used to obtain the existence result for global strong solutions. For an example of the compactness techniques, we refer the reader to [24].

Notice that the condition  $3 \leq m < 4$  is needed for the uniform lower and upper bound estimates in (3.2). If only local time existence of the strong solutions is considered, then the upper and lower bounds in (3.2) can be easily obtained with an extended range for the exponents  $m$  and  $n$ . Therefore we state the existence result for local strong solutions to the model (1.1) with exponents  $m \geq 0, n \geq 0$  as a byproduct in Theorem 2.

**Theorem 2 (Local Existence).** Under the same conditions of Theorem 1, except that the range of the exponents  $(m, n)$  is assumed to be  $m \geq 0, n \geq 0$ , there exists  $T_m > 0$  which depends on  $\eta, \lambda, \|h_0\|_1, \|h_0 s_0\|_1$  and  $\|\bar{S}\|_\infty$ , and unique solutions  $h(x, t) \in L^\infty([0, T_m]; H^k([0, L])) \cap L^2([0, T_m]; H^{k+2}([0, L]))$  and  $s(x, t) \in L^\infty([0, T_m]; H^{k-2}([0, L])) \cap L^2([0, T_m]; H^{k-1}([0, L]))$  that satisfy (1.1ab) with the initial data  $h_0, s_0$  and the boundary conditions (1.1c). Moreover,

$$0 < \lambda \leq s(x, t) \leq \|\bar{S}\|_\infty \quad \text{for all } t \in [0, T_m]. \quad (3.3)$$

Furthermore, there exist positive bounds  $h_m(T_m)$ ,  $H_m(T_m)$  such that

$$0 < h_m(T_m) \leq h(x, t) \leq H_m(T_m) \quad \text{for all } t \in [0, T_m], \quad (3.4)$$

where  $h_m, H_m$  depend on  $\eta, \lambda, \|h_0\|_1, \|h_0 s_0\|_1, \|\bar{S}\|_\infty$  and  $T_m$ .  $\diamond$

For the proof of the main result in Theorem 1, the key point is to obtain the positive upper and lower bounds for  $h$ , which are shown in Steps 1 and 2, respectively. For the following analysis, we denote  $\|\cdot\|_p$  as the standard norm for  $L^p([0, L])$  where  $p \geq 1$ .

The strategy of the proof can be sketched as follows. In Step 1 we get some apriori estimates under the assumption that  $h \geq 0$  and obtain the upper bound  $H_m(T)$  which requires  $m < 4$ . Then we verify the apriori assumption by obtaining a positive lower bound  $h_m(T)$  of  $h$  in Step 2, where  $m \geq 3$  is needed. In Step 3, we use the lower bound  $h_m(T)$  to obtain higher order apriori estimates. After these apriori estimates in the first three steps, following [24, Chapter 10] we apply a standard compactness argument to obtain the existence of strong solutions, which will be described in Remark 1. In Step 4, we prove that the solutions obtained above are unique.

In this following proof we will omit the technical details of the standard compactness argument, and focus on the Steps 1, 2 and 3 for the estimates of the solutions.

**Proof of Theorem 1.**

**Step 1: Basic apriori estimates.**

For the case  $n = m + 1$ , the original model (1.1) can be rewritten as

$$h_t = -h^m(\bar{S} - s) - (h^{m+1}h_{xxx})_x, \quad (3.5a)$$

$$s_t = s_{xx} + \left(\frac{h_x}{h} - h^m h_{xxx}\right)s_x + s(\bar{S} - s)h^{m-1}, \quad (3.5b)$$

with a single system parameter  $m$ .

For any  $T > 0$ , we assume that

$$h(x, t) \geq 0 \quad \text{for all } t \in [0, T]. \quad (3.6)$$

Using this assumption and the initial condition  $\lambda \leq s_0(x) \leq \|\bar{S}(x)\|_\infty$ , we conclude that if  $s = \lambda$  or  $s = \|\bar{S}(x)\|_\infty$  for the first time at  $t = t_c$  at a point  $x = x_c$ , then  $s_x(x_c, t_c) = 0$  is attained. For the last term on the right hand side of (3.5b), we have

$$\begin{aligned} s(\bar{S} - s)h^{m-1}|_{s=\lambda} &= \lambda(\bar{S} - \lambda)h^{m-1} \geq 0, \\ s(\bar{S} - s)h^{m-1}|_{s=\|\bar{S}(x)\|_\infty} &= \|\bar{S}(x)\|_\infty(\bar{S} - \|\bar{S}(x)\|_\infty)h^{m-1} \leq 0. \end{aligned}$$

Then from (3.5b) and the weak maximum principle,  $\lambda \leq s_0(x) \leq \|\bar{S}(x)\|_\infty$  implies that

$$\lambda \leq s(x, t) \leq \|\bar{S}(x)\|_\infty, \quad (3.7)$$

which gives the bounds in (3.1). This estimate together with (1.2) and (1.3) shows that

$$\int_0^L h \, dx \leq C(\|h_0 s_0\|_1, \lambda) \quad \text{for any } t \in [0, T], \quad (3.8)$$

and

$$\int_0^T \int_0^L h^m(\bar{S} - s) \, dx \, dt \leq C(\|h_0\|_1). \quad (3.9)$$

Moreover, multiplying (3.5a) by  $\frac{1-m}{h^m}$  and integrating by parts lead to

$$\begin{aligned} \frac{d}{dt} \int_0^L \frac{1}{h^{m-1}} \, dx &= (m-1) \\ &\times \int_0^L (\bar{S} - s) \, dx - m(m-1) \int_0^L h_{xx}^2 \, dx. \end{aligned} \quad (3.10)$$

From (3.7) and (3.10), we know

$$\int_0^T \int_0^L h_{xx}^2 \, dx \, dt \leq C_\eta + C_s T, \quad (3.11)$$

and

$$\int_0^L \frac{1}{h^{m-1}} \, dx \leq C_\eta + C_s T \quad \text{for any } t \in [0, T], \quad (3.12)$$

where  $C_\eta = \frac{1}{\eta^{m-1}}$ , and  $C_s$  is a constant depending only on  $\|\bar{S}\|_\infty$ .

Furthermore, in order to estimate  $\|h\|_\infty$  and  $\|h_x\|_{L^\infty([0,T];L^2([0,L])}$ , we need another apriori assumption

$$\|h\|_\infty \leq H, \quad (3.13)$$

where  $H$  will be determined later. Multiplying (3.5a) by  $-h_{xx}$  and integrating by parts lead to

$$\frac{d}{dt} \int_0^L \frac{1}{2} h_x^2 \, dx = \int_0^L h^m h_{xx}(\bar{S} - s) \, dx - \int_0^L h_{xxx}^2 h^{m+1} \, dx.$$

Thus by Young's inequality and (3.11), we have

$$\begin{aligned} \int_0^L \frac{1}{2} h_x^2 \, dx &\leq \int_0^T \int_0^L h^m h_{xx}(\bar{S} - s) \, dx \, dt, \\ &\leq \int_0^T \int_0^L h_{xx}^2 \, dx \, dt + \int_0^T \int_0^L h^{2m}(\bar{S} - s)^2 \, dx \, dt, \\ &\leq C_\eta + C_s T + I \quad \text{for any } t \in [0, T], \end{aligned} \quad (3.14)$$

where  $I := \int_0^T \int_0^L h^{2m}(\bar{S} - s)^2 \, dx \, dt$  will be given further treatment.

We introduce two constants  $\kappa, \gamma$  whose values will be determined later and assume that  $m, \kappa, \gamma \geq 1$  satisfy

$$\frac{1}{m} + \frac{1}{\kappa} + \frac{1}{\gamma} = 1. \quad (3.15)$$

Then by Hölder's inequality and (3.8), we have

$$\begin{aligned} \int_0^L h^{2m}(\bar{S} - s)^2 \, dx &= \int_0^L [h^m(\bar{S} - s)]^{\frac{1}{m}} h^{2m-1-\frac{1}{\kappa}}(\bar{S} - s)^{2-\frac{1}{m}} h^{\frac{1}{\kappa}} \, dx \\ &\leq C(\|h_0 s_0\|_1, \lambda) \left( \int_0^L h^m(\bar{S} - s) \, dx \right)^{\frac{1}{m}} \\ &\quad \times \left( \int_0^L h^{(2m-1-\frac{1}{\kappa})\gamma} \, dx \right)^{\frac{1}{\gamma}}. \end{aligned}$$

This, together with Hölder's inequality and (3.9), shows that

$$\begin{aligned} I &\leq C(\|h_0 s_0\|_1, \lambda) \left[ \int_0^T \int_0^L h^m(\bar{S} - s) \, dx \, dt \right]^{\frac{1}{m}} \\ &\quad \times \left[ \int_0^T \left( \int_0^L h^{(2m-1-\frac{1}{\kappa})\gamma} \, dx \right)^{\frac{m'}{\gamma}} \, dt \right]^{\frac{1}{m'}} \\ &\leq C(h_0, s_0) \left[ \int_0^T \left( \int_0^L h^{(2m-1-\frac{1}{\kappa})\gamma} \, dx \right)^{\frac{m'}{\gamma}} \, dt \right]^{\frac{1}{m'}}, \end{aligned} \quad (3.16)$$

where  $m' \geq 1$  satisfies

$$\frac{1}{m} + \frac{1}{m'} = 1. \quad (3.17)$$

Also here and in the following,  $C(h_0, s_0)$  represents a constant depending on  $\|h_0 s_0\|_1, \|h_0\|_1$  and  $\lambda$ .

For any constant  $0 \leq \tau < 2$ , from the apriori assumption (3.13) and (3.16) we have

$$I \leq H^\tau C(\|h_0 s_0\|_1, \lambda) \left[ \int_0^T \left( \int_0^L h^{(2m-1-\frac{1}{\kappa}-\tau)\gamma} \, dx \right)^{\frac{m'}{\gamma}} \, dt \right]^{\frac{1}{m'}}. \quad (3.18)$$

On one hand, from the Gagliardo–Nirenberg interpolation inequality, we know

$$\begin{aligned} \|h\|_{(2m-1-\frac{1}{\kappa}-\tau)\gamma} &\leq c \|h\|_1^{1-\theta} \|h_{xx}\|_2^\theta + c \|h\|_1, \\ &\leq C(h_0, s_0) \|h_{xx}\|_2^\theta + C(h_0, s_0) \\ &\quad \text{for any } t \in [0, T], \end{aligned} \quad (3.19)$$

where the index  $\theta$  satisfies

$$\theta = \frac{2}{5} \left[ 1 - \frac{1}{(2m-1-\frac{1}{\kappa}-\tau)\gamma} \right]. \quad (3.20)$$



On the other hand, from the relations (3.15) and (3.17) we have  $0 \leq \frac{m'}{\gamma} \leq 1$ . Therefore, from (3.18) and (3.19) we obtain

$$I \leq H^\tau C(h_0, s_0) \left[ \left( \int_0^T \|h_{xx}\|_2^{\theta m' (2m-1-\frac{1}{\kappa}-\tau)} dt \right)^{\frac{1}{m'}} + 1 \right]. \quad (3.21)$$

Since we have the uniform bound (3.11), it remains to show that the exponent in (3.21) satisfies

$$\theta m' \left( 2m - 1 - \frac{1}{\kappa} - \tau \right) < 2. \quad (3.22)$$

With the relations (3.15), (3.17) and (3.20), this reduces to

$$\frac{m}{m-1} \left[ \left( 2m - 1 - \frac{1}{\kappa} - \tau \right) - \left( 1 - \frac{1}{m} - \frac{1}{\kappa} \right) \right] < 5, \quad (3.23)$$

which can be rewritten in the following three possible cases,

$$\begin{cases} \text{Case 1: } \frac{6-m}{6-2m+\tau} < m, \quad 6-2m+\tau > 0; & \text{or} \\ \text{Case 2: } m < \frac{6-m}{6-2m+\tau}, \quad 6-2m+\tau < 0; & \text{or} \\ \text{Case 3: } 6-m < 0, \quad 6-2m+\tau = 0. \end{cases} \quad (3.24)$$

Since  $m > 1$  and  $0 \leq \tau < 2$ , only Case 1 can happen, which becomes the minimum requirement to guarantee the condition (3.22),

$$m < 3 + \frac{\tau}{2}. \quad (3.25)$$

Thus we rewrite (3.21) as

$$I \leq C(h_0, s_0) H^\tau. \quad (3.26)$$

This result, together with (3.14), gives

$$\int_0^L h_x^2 dx \leq C_\eta + C_s T + C(h_0, s_0) H^\tau \quad \text{for any } t \in [0, T], \quad (3.27)$$

from which we also know that  $h$  is continuous. Assume that  $h$  attains its minimal value  $h_{\min}$  at  $x = x_c$ . Since (3.8) shows that  $h_{\min} \leq C(h_0, s_0)$ , from (3.27) we have

$$\begin{aligned} \|h\|_\infty &\leq \left| \int_{x_c}^x h_x(s) ds \right| + h_{\min} \\ &\leq \sqrt{C_\eta + C_s T + C(h_0, s_0) H^\tau} + C(h_0, s_0) \\ &\quad \text{for any } t \in [0, T]. \end{aligned} \quad (3.28)$$

Finally, we verify the apriori assumption (3.13). Let us choose  $H$  to be the solution of

$$H = \sqrt{C_\eta + C_s T + C(h_0, s_0) H^\tau} + C(h_0, s_0) + 1. \quad (3.29)$$

In fact, since  $\tau < 2$ , this equation always has a solution,  $H_m(T)$ , which depends on  $C_\eta$ ,  $C(h_0, s_0)$ ,  $C_s$  and  $T$ . Then from (3.28), we have

$$\|h\|_\infty \leq \sqrt{C_\eta + C_s T + C(h_0, s_0) H^\tau} + C(h_0, s_0) < H_m(T) \quad \text{for any } t \in [0, T],$$

which verifies the apriori assumption (3.13). Besides, for any  $m < 4$  there exists  $\delta > 0$  such that  $m < 4 - \delta$ . Then we can choose  $2 - 2\delta < \tau < 2$ , which implies that  $m < 4 - \delta < 3 + \frac{\tau}{2}$ . Therefore we obtain

$$\|h_x\|_{L^\infty([0,T];L^2([0,L]))} \leq C_{h_0,s_0,T}, \quad (3.30)$$

and

$$\|h\|_{L^\infty([0,T] \times [0,L])} \leq H_m(T). \quad (3.31)$$

Here and in the following, we use the notation  $C_{h_0,s_0,T}$  to represent a constant that depends on  $\eta$ ,  $\|h_0\|_1$ ,  $\|\bar{S}\|_\infty$  and  $T$ .

**Step 2: Positive lower bound for  $h$ .**

First from (3.30), (3.31) and the Sobolev embedding  $H^1([0, L]) \hookrightarrow C^{\frac{1}{2}}([0, L])$ , we know

$$h(x) \leq h_{\min} + C_{h_0,s_0,T} |x - x_c|^{\frac{1}{2}}. \quad (3.32)$$

This, together with (3.12), shows that

$$\begin{aligned} &\int_0^L \frac{1}{(h_{\min} + C_{h_0,s_0,T} |x - x_c|^{\frac{1}{2}})^{m-1}} dx \\ &\leq \int_0^L \frac{1}{h^{m-1}} dx \leq C_\eta + C_s T \quad \text{for any } t \in [0, T]. \end{aligned} \quad (3.33)$$

In particular, for  $m = 3$  we have

$$\ln \left( \frac{h_{\min}^2 + C_{h_0,s_0,T}}{h_{\min}^2} \right) = \int_0^{\frac{1}{2}} \frac{1}{h_{\min}^2 + C_{h_0,s_0,T} x} dx \leq 2C_\eta + 2C_s T.$$

Hence we have

$$1 + \frac{C_{h_0,s_0,T}}{h_{\min}^2} \leq e^{2C_\eta + 2C_s T},$$

which leads to

$$h_{\min} \geq \left( \frac{C_{h_0,s_0,T}}{e^{2C_\eta + 2C_s T} - 1} \right)^{\frac{1}{2}}. \quad (3.34)$$

For  $m > 3$ , we have

$$\begin{aligned} \frac{\varepsilon}{(h_{\min} + C_{h_0,s_0,T} \varepsilon^{\frac{1}{2}})^{m-1}} &\leq \int_0^\varepsilon \frac{1}{(h_{\min} + C_{h_0,s_0,T} x^{\frac{1}{2}})^{m-1}} dx \\ &\leq 2C_\eta + 2C_s T, \end{aligned}$$

which gives

$$h_{\min} \geq \left( \frac{\varepsilon}{2C_\eta + 2C_s T} \right)^{\frac{1}{m-1}} - C_{h_0,s_0,T} \varepsilon^{\frac{1}{2}}. \quad (3.35)$$

Since  $\frac{1}{m-1} < \frac{1}{2}$ , we can choose  $\varepsilon$  small enough such that

$\left( \frac{\varepsilon}{2C_\eta + 2C_s T} \right)^{\frac{1}{m-1}} - C_{h_0,s_0,T} \varepsilon^{\frac{1}{2}} > 0$ . Combining the above two cases, we know that for  $m \geq 3$  there exist a positive  $h_m(T) > 0$  depending on  $\eta$ ,  $\|h_0\|_1$ ,  $\|\bar{S}\|_\infty$  and  $T$  such that

$$h(x, t) \geq h_m(T) > 0 \quad \text{for any } t \in [0, T],$$

which gives (3.2) and verifies the apriori assumption (3.6).

**Step 3: Higher order apriori estimates.**

Now we can use (3.2) to obtain higher order estimates. First, we provide an estimate for  $\|h_{xx}\|_{L^\infty([0,T],L^2([0,L]))}$ . With the notation  $h^{(k)} := \frac{\partial^k h}{\partial x^k}$ , we multiply (3.5a) by  $h^{(4)}$  and integrate by parts. From Young's inequality, we have

$$\begin{aligned} \frac{d}{dt} \int_0^L \frac{1}{2} h_{xx}^2 dx &= - \int_0^L h^m (\bar{S} - s) h^{(4)} \\ &\quad + h^{m+1} (h^{(4)})^2 + (h^{m+1})_x h_{xxx} h^{(4)} dx \\ &\leq \int_0^L -h^{m+1} (h^{(4)})^2 + \varepsilon (h^{(4)})^2 \\ &\quad + c(\varepsilon) H_m^{2m} \|\bar{S}\|_\infty^2 dx + I_1, \end{aligned} \quad (3.36)$$

where  $I_1 := -\int_0^L (h^{m+1})_x h_{xxx} h^{(4)} dx$ . Our goal is to use  $-\int_0^L h_m^{m+1} (h^{(4)})^2 dx$  to control  $I_1$  based on the inequality

$$\begin{aligned} I_1 &= -\frac{1}{2} \int_0^L (h^{m+1})_x (h_{xxx}^2)_x dx = \frac{1}{2} \int_0^L (h^{m+1})_{xx} h_{xxx}^2 dx \\ &\leq C(H_m) \int_0^L h_{xx} h_{xxx}^2 dx + C(H_m) \int_0^L h_x^2 h_{xxx}^2 dx =: I_2 + I_3. \end{aligned}$$

With the uniform bound (3.30), we use the Gagliardo–Nirenberg interpolation inequality to estimate  $I_2, I_3$ . For  $I_2$ , we obtain

$$\|h_{xx}\|_\infty \leq \|h_x\|_2^{1-\theta_2} \|h^{(4)}\|_2^{\theta_2} + C_{h_0, s_0, T} \quad \text{for } \theta_2 = \frac{1}{2}, \quad (3.37)$$

and

$$\|h_{xxx}\|_2 \leq \|h_x\|_2^{1-\theta_1} \|h^{(4)}\|_2^{\theta_1} + C_{h_0, s_0, T} \quad \text{for } \theta_1 = \frac{2}{3}. \quad (3.38)$$

Since  $\theta_2 + 2\theta_1 = \frac{11}{6} < 2$ , the estimates (3.37) and (3.38) together with Young's inequality yield that

$$I_2 \leq C(H_m) \|h_{xx}\|_\infty \|h_{xxx}\|_2^2 \leq \varepsilon \|h^{(4)}\|_2^2 + C_{h_0, s_0, T}. \quad (3.39)$$

Similarly, for  $I_3$  we obtain

$$\|h_x\|_\infty \leq \|h_x\|_2^{1-\theta_4} \|h^{(4)}\|_2^{\theta_4} + C_{h_0, s_0, T} \quad \text{for } \theta_4 = \frac{1}{6}, \quad (3.40)$$

and

$$\|h_{xxx}\|_2 \leq \|h_x\|_2^{1-\theta_3} \|h^{(4)}\|_2^{\theta_3} + C_{h_0, s_0, T} \quad \text{for } \theta_3 = \frac{2}{3}. \quad (3.41)$$

With  $2\theta_3 + 2\theta_4 = \frac{5}{3} < 2$ , using (3.40) and (3.41) with Young's inequality leads to

$$I_3 \leq C(H_m) \|h_x\|_\infty^2 \|h_{xxx}\|_2^2 \leq \varepsilon \|h^{(4)}\|_2^2 + C_{h_0, s_0, T}. \quad (3.42)$$

Combining (3.39) and (3.42) with (3.36), we have

$$\frac{d}{dt} \int_0^L h_{xx}^2 dx + \int_0^L h_m^{m+1} (h^{(4)})^2 dx \leq C_{h_0, s_0, T}, \quad (3.43)$$

which gives that

$$\|h_{xx}\|_{L^\infty([0, T], L^2([0, L]))} \leq C_{h_0, s_0, T}, \quad (3.44)$$

$$\|h^{(4)}\|_{L^2([0, T], L^2([0, L]))} \leq C_{h_0, s_0, T}. \quad (3.45)$$

Second, in order to get higher order estimates for  $h$ , we now need to obtain some estimates for  $s$ . Multiplying (3.5b) by  $s$  and applying integration by parts, we have

$$\begin{aligned} \frac{d}{dt} \int_0^L \frac{1}{2} s^2 dx &= -\int_0^L s_x^2 dx + \int_0^L \left( \frac{h_x}{h} - h^m h_{xxx} \right) s s_x \\ &\quad + s^2 (\bar{s} - s) h^{m-1} dx \\ &\leq -\int_0^L s_x^2 dx + \varepsilon \int_0^L s_x^2 dx + C(\varepsilon, \|\bar{s}\|_\infty) \\ &\quad \times \int_0^L \left( \frac{h_x}{h} - h^m h_{xxx} \right)^2 dx + \int_0^L s^2 (\bar{s} - s) h^{m-1} dx \\ &\leq -\int_0^L s_x^2 dx + \varepsilon \int_0^L s_x^2 dx + C(\varepsilon, \|\bar{s}\|_\infty) \\ &\quad \times \int_0^L \left( 2 \frac{(h_x)^2}{h^2} + 2 h_m^{2m} (h_{xxx})^2 \right) dx + C_{h_0, s_0, T}, \end{aligned} \quad (3.46)$$

where Young's inequality and (3.2) are used. With the estimates (3.44) and (3.45), we integrate (3.46) from  $t = 0$  to  $t = T$  and

obtain

$$\begin{aligned} \int_0^L s^2 dx + \int_0^T \int_0^L s_x^2 dx &\leq C_{h_0, s_0, T} \\ \text{for any } t \in [0, T]. \end{aligned} \quad (3.47)$$

Third, we turn to estimate  $\|h_{xxx}\|_{L^\infty([0, T], L^2([0, L]))}$ . Multiplying (3.5a) by  $h^{(6)}$  and applying integration by parts, we have

$$\begin{aligned} \frac{d}{dt} \int_0^L \frac{1}{2} h_{xxx}^2 dx &= \int_0^L h^m (\bar{s} - s) h^{(6)} - (h^{m+1} h_{xxx})_{xx} h^{(5)} dx \\ &= -\int_0^L (h^m (\bar{s} - s))_x h^{(5)} dx - \int_0^L h^{m+1} (h^{(5)})^2 dx \\ &\quad - \int_0^L 2(h^{m+1})_x h^{(4)} h^{(5)} + (h^{m+1})_{xx} h_{xxx} h^{(5)} dx \\ &\leq \varepsilon \int_0^L (h^{(5)})^2 dx + C(\varepsilon) C_{h_0, s_0, T} - \int_0^L h_m^{m+1} (h^{(5)})^2 dx \\ &\quad + \int_0^L (h^{m+1})_{xx} (h^{(4)})^2 dx - \int_0^L (h^{m+1})_{xx} h_{xxx} h^{(5)} dx, \end{aligned} \quad (3.48)$$

where Young's inequality, (3.2), (3.30) and (3.47) are used in the last inequality.

We then introduce  $R := \int_0^L (h^{m+1})_{xx} (h^{(4)})^2 dx$  and  $R_3 := -\int_0^L (h^{m+1})_{xx} h_{xxx} h^{(5)} dx$ , and write

$$\begin{aligned} R &= \int_0^L (h^{m+1})_{xx} (h^{(4)})^2 dx \\ &\leq C(H_m) \int_0^L h_{xx} (h^{(4)})^2 dx + C(H_m) \int_0^L h_x^2 (h^{(4)})^2 dx \\ &=: R_1 + R_2. \end{aligned}$$

It will be shown that the term  $-\int_0^L h_m^{m+1} (h^{(5)})^2 dx$  can be used to control the terms  $R_1, R_2$  and  $R_3$ .

For  $R_1$ , using the Gagliardo–Nirenberg interpolation inequality and keeping in mind that the uniform bound (3.44), we obtain

$$\|h_{xx}\|_\infty \leq \|h_{xx}\|_2^{1-\theta_2} \|h_{xxx}\|_2^{\theta_2} + C_{h_0, s_0, T} \quad \text{for } \theta_2 = \frac{1}{2}, \quad (3.49)$$

and

$$\|h^{(5)}\|_2 \leq \|h_{xx}\|_2^{1-\theta_1} \|h^{(5)}\|_2^{\theta_1} + C_{h_0, s_0, T} \quad \text{for } \theta_1 = \frac{2}{3}. \quad (3.50)$$

Then (3.49) and (3.50) show that

$$\begin{aligned} R_1 &\leq C(H_m) \|h_{xx}\|_\infty \|h^{(4)}\|_2^2 \\ &\leq C_{h_0, s_0, T} \|h_{xxx}\|_2^{\theta_2} \|h^{(5)}\|_2^{2\theta_1} + C_{h_0, s_0, T} \|h_{xxx}\|_2^{\theta_2} \\ &\quad + C_{h_0, s_0, T} \|h^{(5)}\|_2^{2\theta_1} + C_{h_0, s_0, T}. \end{aligned} \quad (3.51)$$

From Young's inequality, we have

$$\|h_{xxx}\|_2^{\theta_2} \|h^{(5)}\|_2^{2\theta_1} \leq \varepsilon \|h^{(5)}\|_2^{2p\theta_1} + C(\varepsilon) \|h_{xxx}\|_2^{q\theta_2},$$

where  $q = 3, p = \frac{3}{2}$ . Since  $q\theta_2, 2\theta_1 < 2$ , applying Young's inequality again, we obtain

$$R_1 \leq \varepsilon \|h^{(5)}\|_2^2 + C_{h_0, s_0, T} \|h_{xxx}\|_2^2 + C_{h_0, s_0, T}. \quad (3.52)$$

For  $R_2$ , using (3.44) and the Sobolev interpolation inequality we have

$$\begin{aligned} R_2 &= C(H_m) \int_0^L h_x^2 (h^{(4)})^2 dx \leq C(H_m) \|h_x\|_\infty^2 \|h^{(4)}\|_2^2 \\ &\leq C(H_m) \|h_{xx}\|_2^2 \|h^{(4)}\|_2^2 \leq C_{h_0, s_0, T} \|h^{(4)}\|_2^2 \\ &\leq \varepsilon \|h^{(5)}\|_2^2 + C_{h_0, s_0, T}. \end{aligned} \quad (3.53)$$

Similarly, for the control of  $R_3$ , from Young's inequality and the Sobolev interpolation inequality we have

$$R_3 = - \int_0^L (h^{m+1})_{xx} h_{xxx} h^{(5)} dx \quad (3.54)$$

$$\begin{aligned} &\leq \varepsilon \|h^{(5)}\|_2^2 + \|h_{xxx}\|_\infty^2 \int_0^L (h^{m+1})_{xx}^2 dx \\ &\leq \varepsilon \|h^{(5)}\|_2^2 + (\varepsilon \|h^{(5)}\|_2^2 + C_{h_0, s_0, T}) (\|h_{xxx}\|_2^2 + \|h_x\|_4^4) \\ &\leq \varepsilon \|h^{(5)}\|_2^2 + C_{h_0, s_0, T}, \end{aligned} \quad (3.55)$$

where (3.44) is used.

Combining (3.52)–(3.54) and (3.48), we obtain

$$\begin{aligned} &\frac{d}{dt} \int_0^L h_{xxx}^2 dx + \int_0^L h_m^{m+1} (h^{(5)})^2 dx \\ &\leq C_{h_0, s_0, T} \|h_{xxx}\|_2^2 + C_{h_0, s_0, T}. \end{aligned} \quad (3.56)$$

This, together with the Grönwall inequality, implies that

$$\|h_{xxx}\|_{L^\infty([0, T], L^2([0, L]))} \leq C_{h_0, s_0, T}, \quad (3.57)$$

$$\|h^{(5)}\|_{L^2([0, T], L^2([0, L]))} \leq C_{h_0, s_0, T}. \quad (3.58)$$

Finally, we consider the estimate for  $\|s_x\|_{L^\infty([0, T], L^2([0, L]))}$ . Multiplying (3.5b) by  $-s_{xx}$ , integrating by parts, and using Young's inequality, (3.7) and (3.2), we have

$$\begin{aligned} &\frac{d}{dt} \int_0^L \frac{1}{2} s_x^2 dx = - \int_0^L s_{xx}^2 + \left( \frac{h_x}{h} - h^m h_{xxx} \right) s_x s_{xx} \\ &\quad + s s_{xx} (\bar{s} - s) h^{m-1} dx \\ &\leq - \int_0^L s_{xx}^2 dx + \varepsilon \int_0^L s_{xx}^2 dx \\ &\quad + \frac{1}{2} \int_0^L \left( \frac{h_x}{h} - h^m h_{xxx} \right)_x s_x^2 dx + C_{h_0, s_0, T}, \end{aligned} \quad (3.59)$$

where the first term on the right hand side will be used to control  $P := \frac{1}{2} \int_0^L \left( \frac{h_x}{h} - h^m h_{xxx} \right)_x s_x^2 dx$ . From (3.30), (3.44) and (3.2), we know that

$$\begin{aligned} P &\leq C_{h_0, s_0, T} \left[ \int_0^L h_{xx} s_x^2 + h_x^2 s_x^2 + h_x h_{xxx} s_x^2 + h^{(4)} s_x^2 dx \right] \\ &\leq C_{h_0, s_0, T} \left[ (\|h_{xx}\|_\infty + \|h_x\|_\infty^2) \int_0^L s_x^2 dx \right. \\ &\quad \left. + \|h_x\|_\infty \int_0^L h_{xxx} s_x^2 dx + \int_0^L h^{(4)} s_x^2 dx \right] \\ &\leq \varepsilon \int_0^L s_{xx}^2 dx + C_{h_0, s_0, T} \left( \int_0^L h_{xxx} s_x^2 dx + \int_0^L h^{(4)} s_x^2 dx \right) \\ &\quad + C_{h_0, s_0, T}. \end{aligned} \quad (3.60)$$

Now we provide an estimate for  $\int_0^L h^{(4)} s_x^2 dx$ , and the other term  $\int_0^L h_{xxx} s_x^2 dx$  can be treated similarly. With  $p = \frac{5}{3}$ , and  $q = \frac{5}{2}$ , we have

$$\int_0^L h^{(4)} s_x^2 dx \leq C(\varepsilon) \int_0^L (h^{(4)})^q dx + \varepsilon \int_0^L s_x^{2p} dx. \quad (3.61)$$

Using the Gagliardo–Nirenberg interpolation inequality and (3.47), we obtain

$$\|s_x\|_{2p} \leq \|s_{xx}\|_2^{\theta_1} \|s\|_2^{1-\theta_1} + C_{h_0, s_0, T} \quad \text{for } \theta_1 = \frac{3}{5}, \quad (3.62)$$

and

$$\|h^{(4)}\|_q \leq \|h^{(5)}\|_2^{\theta_2} \|h_{xxx}\|_2^{1-\theta_2} + C_{h_0, s_0, T} \quad \text{for } \theta_2 = \frac{11}{20}. \quad (3.63)$$

Thus we have

$$\int_0^L s_x^{2p} dx \leq C_{h_0, s_0, T} \int_0^L s_{xx}^2 dx + C_{h_0, s_0, T}, \quad (3.64)$$

and since  $q\theta_2 = \frac{55}{40} < 2$ , we know

$$\int_0^L (h^{(4)})^q dx \leq C_{h_0, s_0, T} \int_0^L (h^{(5)})^2 dx + C_{h_0, s_0, T}. \quad (3.65)$$

Therefore, combining (3.62), (3.64) and (3.65) with (3.60), we have

$$P \leq \varepsilon \int_0^L s_{xx}^2 dx + C_{h_0, s_0, T} \int_0^L (h^{(5)})^2 dx + C_{h_0, s_0, T}.$$

This, together with (3.59), gives

$$\begin{aligned} &\frac{d}{dt} \int_0^L s_x^2 dx + \int_0^L s_{xx}^2 dx \\ &\leq C_{h_0, s_0, T} \int_0^L (h^{(5)})^2 dx + C_{h_0, s_0, T}. \end{aligned} \quad (3.66)$$

Using (3.58) and integrating (3.66) in time from  $t = 0$  to  $t = T$ , we obtain

$$\|s_x\|_{L^\infty([0, T], L^2([0, L]))} \leq C_{h_0, s_0, T}, \quad (3.67)$$

$$\|s_{xx}\|_{L^2([0, T], L^2([0, L]))} \leq C_{h_0, s_0, T}. \quad (3.68)$$

We can use the same techniques to obtain any  $k$ th order estimates, for which we omit the details. Then by standard compactness arguments, we can obtain the existence result for global solutions to (3.5).

**Step 4: Uniqueness of the solutions obtained above.**

Assume that  $(h_1, s_1)$ ,  $(h_2, s_2)$  are two strong solutions that satisfy the Eqs. (3.5). Let us first estimate  $\frac{d}{dt} \|h_1 - h_2\|_2^2$ . Taking the difference between (3.5a) for  $h_1$  and  $h_2$ , we write

$$\begin{aligned} (h_1 - h_2)_t &= -h_1^m (\bar{s} - s_1) + h_2^m (\bar{s} - s_2) \\ &\quad - (h_1^{m+1} h_{1xxx} - h_2^{m+1} h_{2xxx})_x. \end{aligned} \quad (3.69)$$

Notice that the strong solutions have the regularities  $h(x, t) \in L^\infty([0, T]; H^k([0, L])) \cap L^2([0, T]; H^{k+2}([0, L]))$  and  $s(x, t) \in L^\infty([0, T]; H^{k-2}([0, L])) \cap L^2([0, T]; H^{k-1}([0, L]))$ . From now on, we denote  $C_{h, s}$  as a constant that depends on  $\|(h_1, h_2)\|_{L^\infty([0, T]; H^k([0, L]))}$ ,  $\|(h_1, h_2)\|_{L^2([0, T]; H^{k+2}([0, L]))}$ ,  $\|(s_1, s_2)\|_{L^\infty([0, T]; H^{k-2}([0, L]))}$  and  $\|(s_1, s_2)\|_{L^2([0, T]; H^{k-1}([0, L]))}$ . Multiplying (3.69) by  $h_1 - h_2$  and applying integration by parts, we have

$$\begin{aligned} &\frac{d}{dt} \int_0^L \frac{1}{2} (h_1 - h_2)^2 dx = \int_0^L (h_2^m - h_1^m) (\bar{s} - s_1) (h_1 - h_2) \\ &\quad + h_2^m (s_1 - s_2) (h_1 - h_2) + (h_1^{m+1} - h_2^{m+1}) h_{1xxx} (h_1 - h_2)_x \\ &\quad + h_2^{m+1} (h_{1xxx} - h_{2xxx}) (h_1 - h_2)_x dx \\ &\leq C_{h, s} \left( \|h_1 - h_2\|_2^2 + \|s_1 - s_2\|_2^2 \right) \\ &\quad + \int_0^L (h_1^{m+1} - h_2^{m+1}) h_{1xxx} (h_1 - h_2)_x \\ &\quad + h_2^{m+1} (h_{1xxx} - h_{2xxx}) (h_1 - h_2)_x dx \\ &\leq C_{h, s} \left( \|h_1 - h_2\|_2^2 + \|s_1 - s_2\|_2^2 \right) \\ &\quad + C_{h, s} \|h_{1xxx}\|_2 \int_0^L (h_{1x} - h_{2x})^2 dx \\ &\quad - \int_0^L h_2^{m+1} (h_{1xx} - h_{2xx})^2 - (h_2^{m+1})_x \\ &\quad \times (h_{1xx} - h_{2xx}) (h_1 - h_2)_x dx \\ &\leq C_{h, s} \left( \|h_1 - h_2\|_2^2 + \|s_1 - s_2\|_2^2 + \|h_{1xxx}\|_2 \|h_{1x} - h_{2x}\|_2^2 \right). \end{aligned} \quad (3.70)$$



Here we used Young's inequality and (3.2) in the last inequality.

Second, we turn to estimate  $\frac{d}{dt} \|h_{1x} - h_{2x}\|_2^2$ . Multiplying (3.69) by  $-(h_1 - h_2)_{xx}$  and applying integration by parts, we obtain

$$\begin{aligned} \frac{d}{dt} \int_0^L \frac{1}{2} (h_{1x} - h_{2x})^2 dx &= - \int_0^L (h_2^m - h_1^m)(\bar{S} - s_1)(h_{1xx} - h_{2xx}) \\ &\quad + h_2^m(s_1 - s_2)(h_{1xx} - h_{2xx}) + h_1^{m+1}(h_{1xxx} - h_{2xxx})^2 \\ &\quad + (h_1^{m+1} - h_2^{m+1})h_{2xxx}(h_{1xxx} - h_{2xxx}) dx \\ &\leq C_{h,s} \left( \|h_1 - h_2\|_2^2 + \|s_1 - s_2\|_2^2 \right) - \int_0^L \frac{1}{2} h_1^{m+1} (h_{1xxx} - h_{2xxx})^2 \\ &\quad + (h_1^{m+1} - h_2^{m+1})h_{2xxx}(h_{1xxx} - h_{2xxx}) dx \\ &\leq C_{h,s} \left( \|h_1 - h_2\|_2^2 + \|s_1 - s_2\|_2^2 \right) \\ &\quad - \frac{1}{4} \int_0^L h_1^{m+1} (h_{1xxx} - h_{2xxx})^2 \\ &\quad + C_{h,s} \|h_{2xxx}\|_2 \|h_1 - h_2\|_\infty^2 dx \\ &\leq C_{h,s} \left( \|h_1 - h_2\|_2^2 + \|s_1 - s_2\|_2^2 + \|h_{2xxx}\|_2 \|h_{1x} - h_{2x}\|_2^2 \right). \end{aligned} \quad (3.71)$$

Young's inequality and (3.2) are also used in the first and second inequalities.

Next, we need to estimate  $\frac{d}{dt} \|h_{1xx} - h_{2xx}\|_2^2$  and  $\frac{d}{dt} \|s_1 - s_2\|_2^2$ . As the involved techniques are identical to those used in the estimates for (3.36) and (3.46) in Step 3, we omit the details here and state that we have the estimate

$$\begin{aligned} \frac{d}{dt} \left( \|h_1 - h_2\|_{H^2([0,L])}^2 + \|s_1 - s_2\|_2^2 \right) \\ \leq C_{h,s} \left( 1 + \|h_1^{(4)}\|_2^2 + \|h_2^{(4)}\|_2^2 \right) \\ \times \left( \|h_1 - h_2\|_{H^2([0,L])}^2 + \|s_1 - s_2\|_2^2 \right). \end{aligned} \quad (3.72)$$

Hence by the Grönwall inequality and the fact that  $h_1(0) = h_2(0)$ ,  $s_1(0) = s_2(0)$ , we have  $h_1 \equiv h_2$  and  $s_1 \equiv s_2$ . This completes the proof of Theorem 1.  $\square$

**Remark 1.** The compactness argument that we use in the proof above can be stated as follows. We first modify (3.5) properly using the standard mollifier  $J_\delta$  such that the right-hand-sides of the modified system are locally Lipschitz continuous in Banach space  $L^\infty([0, L])$ , so that the Picard Theorem for the abstract Banach space can be applied. Hence by [24, Theorem 3.1], the modified system has a unique local solution  $(h_\delta, s_\delta)$ . Then by the apriori estimates in Steps 1, 2 and 3, we get the regularity estimates uniformly in  $\delta$  and extend the maximal existence time for  $(h_\delta, s_\delta)$ . Finally, by the Lions–Aubin compactness lemma and taking the limit  $\delta \rightarrow 0$ , we obtain a solution  $(h, s)$  to the original problem (3.5).

**Remark 2.** A sketch of the proof of Theorem 2 is presented here. Recall that in Theorem 1 the condition  $m < 4$  comes from the upper bound  $H_m(T)$  and that the condition  $3 \leq m$  is used to obtain the lower bound  $h_m(T)$ . However, for local solutions we can obtain the apriori boundedness estimate (3.2) easily for any  $m \geq 0$ . Thus the techniques for apriori estimates and compactness argument are the same as the proof of Theorem 1 and we omit the details here.

#### 4. Dynamics of model (1.1): numerical study

It was analytically shown in the previous section that for parameters  $n = m + 1$  and  $3 \leq m < 4$  global solutions to (1.1) exist. In this section, we conduct a series of numerical simulations for the generalized Eqs. (1.1) with different values of mobility exponents  $(m, n)$  to further investigate various long-time

behaviors of the solutions. Moreover, simulations reveal that the model has rich dynamics resulting from its strong nonlinearity. For example, interesting finite-time singularities are observed with  $(m, n) = (0, 3)$  which corresponds to the original tear film break up model (2.10). We will also discuss the significance of the effective salt capacity  $\bar{S}(x)$  to the existence of equilibrium solutions and the dynamics of the model.

##### 4.1. Finite-time singularities

While the motivating tear film break-up model (2.10) successfully captures the key components in evaporating tear films, the instabilities driven by the locally elevated evaporation rates can lead to a novel finite-time rupture–shock phenomenon. Fig. 2 shows a typical numerical simulation for the evolution of film height and osmolarity from initial condition  $h_0 = s_0 = 1$  with  $\bar{S}$  given by  $\bar{S}(x) = 50 - 48.8 \tanh(20(|x - 1| - 0.1))$ .

In the early stage of the dynamics, it is shown in Fig. 2(a, b) that the film thickness  $h$  decreases with the osmolarity  $s$  increasing since the locally elevated evaporation effects are large enough to overcome the curvature-driven and osmotic healing flows. In the later stage, Fig. 2(d) shows that  $s$  locally exceeds the prescribed  $\bar{S}$ , and the local minimum of  $h$  splits into a pair of local minimums that lead to secondary rupture (see Fig. 2(c)); at the same time the rupture in  $h$  is smoothed by both weak diffusive and capillary forces. As thinning proceeds, the film thickness in the neighborhood of the critical position  $x_c$  approaches zero which leads to degenerate diffusion for the local salt concentration from (2.4). This causes the osmolarity to form a singular shock in finite-time with  $|s_x(x_c, t)| \rightarrow \infty$  for  $t \rightarrow t_c$  (see Fig. 2(f)) with the development of tear film rupture as  $h(x_c, t) \rightarrow 0$  (see Fig. 2(e)). It is clear from Fig. 2(d) that the osmolarity  $s$  is bounded by  $\|\bar{S}\|_\infty$  throughout the simulation as is predicted by (3.1).

This type of rupture–shock dynamics is comparable to the double shock solutions studied in [25,26] in a model for a thin viscous film with insoluble surfactant. That PDE system for film thickness  $h$  and surfactant concentration  $\Gamma$  allows shock solutions for which both  $h$  and  $\Gamma_x$  have a jump while  $\Gamma$  is continuous. In particular, Jensen and Grotberg [25] showed that severe film thinning behind the shock due to van der Waals can lead to film rupture. Different double shock and singular shock solutions for film thickness and particle volume fraction have also been investigated by Cook and Bertozzi for particle-laden thin films [13].

The nonlinear PDE system (1.1) is solved numerically using a fully implicit second-order finite difference method with an adaptive non-uniform grid. Specifically, we used the midpoint Keller-box method [27] to express the PDEs as a system of first-order equations

$$h_t = -(h^n q)_x - h^m(\bar{S} - s) \quad (hs)_t = (hv - h^n qs)_x, \quad (4.1a)$$

with

$$v = s_x, \quad k = h_x, \quad p = k_x, \quad q = p_x, \quad (4.1b)$$

where the second equation in (4.1a) maintains the conservation of local salt mass from Eq. (2.4). To capture the finite-time rupture in  $h$  and shock in  $s$  that occur simultaneously with high resolutions, we used a classical moving mesh algorithm with a tailored monitor function together with adaptive time-stepping to adaptively assign a high distribution of grid points near the singularity points. For more discussion and applications of moving mesh methods, we refer readers to [28].

The presence of finite-time singularities indicates that the tear film model (2.10) is problematic since the solution  $(h, s)$  cannot be continued past the time of the first singularity. Our regularization of the non-conservative contributions by introducing the mobility parameter  $m$  to the generalized model (1.1) is inspired by this

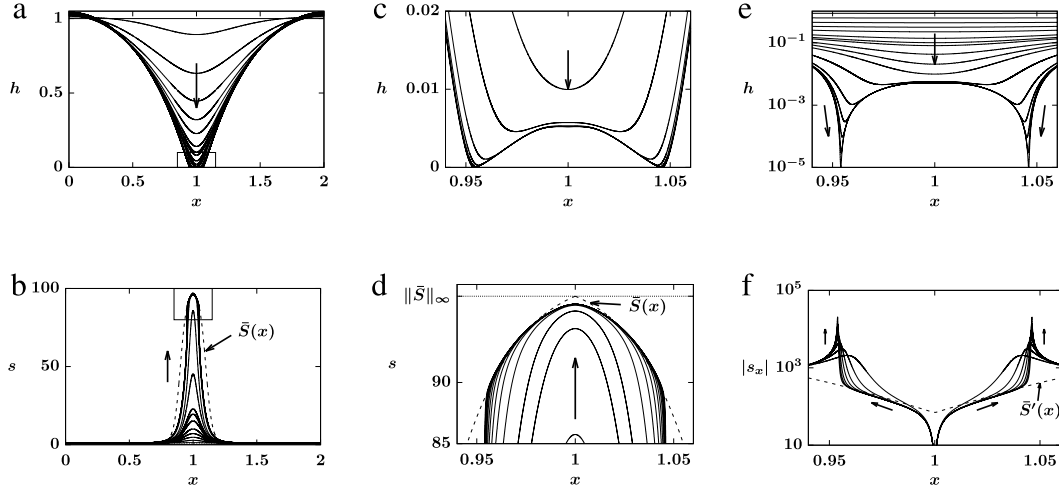


**Fig. 2.** Evolution of  $h$  and  $s$  in Eqs. (2.10ab) with  $\epsilon = 0$ , or equivalently, Eqs. (1.1ab) with  $(m, n) = (0, 3)$ , starting from constant initial data  $h_0 = s_0 = 1$  for  $0 \leq x \leq 2$  driven by the non-conservative flux with  $\bar{S}(x) = 50 - 48.8 \tanh(20(|x - 1| - 0.1))$  (plotted in dashed lines in (b, d)). Solution profiles for  $h$  and  $s$  are shown in (a) and (b), with zoom-in plots in (c) and (d). In (e) and (f) solutions  $h$  and  $|s_x|$  are plotted on log scale, showing a finite time rupture–shock singularity occurring at  $x_c$  with  $h(x_c) \rightarrow 0$  and  $|s_x(x_c)| \rightarrow \infty$  as  $t \rightarrow t_c$ .

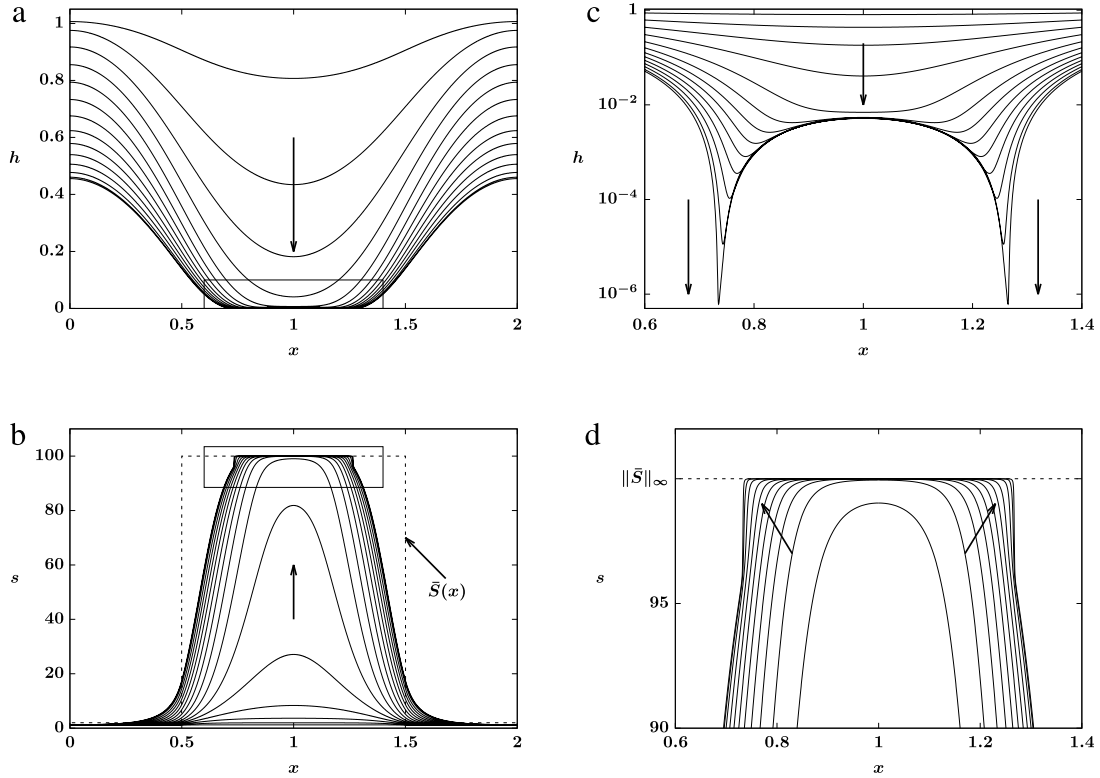


**Fig. 3.** Numerical simulation of (1.1) with  $(m, n) = (1/2, 3/2)$  and identical initial data and  $\bar{S}$  (in dashed lines), (4.2) with  $w = 0.5$ , as in Fig. 1. Evolution of  $h$  and  $s$  are plotted in (a) and (b), with zoom-in plots in (c) and (d) showing that rupture–shock singularity occurs at a pair of points  $x_c$  away from  $x = 1$  with  $h(x_c) \rightarrow 0$  and  $|s_x(x_c)| \rightarrow \infty$  as  $t \rightarrow t_c$ , where  $t_c \approx 0.063$ .

observation. For the following simulations we keep  $n = m + 1$  so that the parameters are consistent with those used in Theorem 1. We also apply the initial conditions  $h_0 = s_0 = 1$  with domain size  $L = 2$ , and define the effective salt capacity  $\bar{S}(x)$  as an indicator function identifying the elevated-evaporation-rate region,

$$\bar{S}(x) = \begin{cases} 100 & \text{for } L/2 - w < x < L/2 + w, \\ 2 & \text{otherwise,} \end{cases} \quad (4.2)$$

where  $w > 0$  gives the half width of the region. This choice of  $\bar{S}$  and initial data satisfy the requirement of the global existence theorem

$s_0 \leq \|\bar{S}\|_\infty$  and provide a typical characterization of the dynamics in the model (2.10).

The PDE simulations shown in Fig. 3 with  $(m, n) = (1/2, 3/2)$  and  $w = 0.5$  suggest that weak regularization is not sufficient to prevent the finite-time singularities from happening. Similar to the dynamics presented in Fig. 2, rupture–shock phenomenon occurs in the later stage with  $h(x_c) \rightarrow 0$  and  $|s_x(x_c)| \rightarrow \infty$  as  $t \rightarrow t_c \approx 0.063$ . Since the width of the high capacity region in  $\bar{S}$  increases from approximately 0.2 in Fig. 2 to width one in Fig. 3, the domain with reduced film thickness and the hyperosmotic region in  $s$  are larger, while the secondary rupture–shock phenomenon

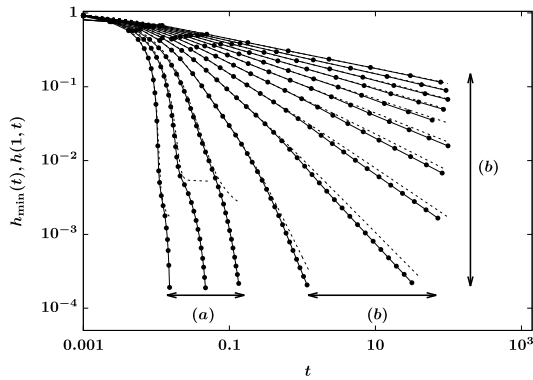


**Fig. 4.** Plot of decreasing minimum film thickness  $h_{\min}$  (plotted in dotted lines) and  $h(1, t)$  (plotted in dashed lines) starting from identical initial condition  $h_0 = s_0 = 1$  with  $n = m + 1$ ,  $\bar{S}$  from (4.2) with  $w = 0.5$  and over a range of  $m$  values,  $0 \leq m \leq 6$ . Regime (a)  $m = 0, 0.5, 1$ ; Regime (b)  $m = 1.5, \dots, 6$ . In regime (a) finite-time rupture in  $h$  occurs, while infinite-time thinning occurs in regime (b). The deviation of  $h_{\min}(t)$  from  $h(1, t)$  in the later stage indicates that the minimum of the film thickness  $h(x, t)$  is attained away from the center of the domain.

that occurs away from the center of the domain is similar to Fig. 2. Again the comparison between the profiles for  $\bar{S}$  and the salt concentration  $s$  in Fig. 3(d) emphasizes that  $s$  does not exceed  $\|\bar{S}\|_{\infty} = 100$  during the dynamical evolution.

Note that the distinct numerical simulations presented in Figs. 1 and 3 differ only in their choices of mobility exponents  $(m, n)$ , with all the other system parameters including the  $\bar{S}$  profile being identical. Inspired by this observation, we explore the dynamics of (1.1) with  $\bar{S}$  given by (4.2) with  $w = 0.5$  and investigate the influences of various mobility exponents  $m$  with  $n = m + 1$ . The time evolution of a set of PDE simulations with identical initial data is plotted in Fig. 4 with two different regimes. For  $0 \leq m \leq 1$ , localized finite-time rupture occurs at a point away from the origin similar to the dynamics shown in Fig. 3, while for  $m > 1$  infinite-time non-uniform thinning is observed with the minimum film thickness  $h_{\min} \rightarrow 0$  as  $t \rightarrow \infty$ , which is similar to the dynamics shown in Fig. 1. Specifically, the film thicknesses at the center of the domain  $x = 1$  are plotted in comparison to the minimum film thickness. For regime (a), as the finite-time singularity develops,  $h_{\min}(t)$  quickly deviates from  $h(1, t)$  and the difference between the two quantities grows exponentially as the critical time is approached, indicating the formation of the secondary singularities similar to the case shown in Fig. 3. These results are in line with the conclusion drawn in Theorem 1 that strong solutions to (1.1) exist globally for  $3 \leq m < 4$  and  $n = m + 1$ , and therefore the numerical treatment is consistent. Moreover, the numerical result in Fig. 3 suggests that solutions to the model (1.1) exist until the first singularity occurs, which agrees with the local solution result in Theorem 2.

#### 4.2. Convergence to equilibrium and infinite time thinning

It is shown in Fig. 4 that with  $\bar{S}(x)$  from (4.2) and  $w = 0.5$  one can separate the finite-time singularity regime of the solution behaviors from infinite-time thinning regime with various  $(m, n)$  values. We will then further investigate the long time behavior of the solutions of (1.1). In addition to the infinite time thinning, typical long-time behaviors of solutions  $(h, s)$  of PDE system (1.1) may also include convergence to equilibrium solutions.

There is a possible equilibrium balance between the regularized non-conservative effects and the surface tension contributions in the PDE system. By setting the time-derivative terms in (1.1) equal to zero, we note that an equilibrium of the PDE system (1.1),  $h_{\text{eq}}(x)$

and  $s_{\text{eq}}(x)$ , satisfies the differential equation system

$$\frac{d}{dx} \left( h_{\text{eq}}^n \frac{d^3 h_{\text{eq}}}{dx^3} \right) + h_{\text{eq}}^m (\bar{S} - s_{\text{eq}}) = 0, \quad (4.3a)$$

$$\frac{d^2 s_{\text{eq}}}{dx^2} + \left( \frac{1}{h_{\text{eq}}} \frac{dh_{\text{eq}}}{dx} - h_{\text{eq}}^{n-1} \frac{d^3 h_{\text{eq}}}{dx^3} \right) \frac{ds_{\text{eq}}}{dx} + s_{\text{eq}} (\bar{S} - s_{\text{eq}}) h_{\text{eq}}^{m-1} = 0, \quad (4.3b)$$

subject to the no-flux and normal-contact boundary conditions

$$\frac{dh_{\text{eq}}}{dx} = 0, \quad \frac{d^3 h_{\text{eq}}}{dx^3} = 0, \quad \frac{ds_{\text{eq}}}{dx} = 0 \quad \text{at } x = 0, L. \quad (4.3c)$$

Due to the conservation of total mass of salt (2.5), another constraint is imposed for the PDE system starting from the initial data  $(h_0, s_0)$ ,

$$\int_0^L h_{\text{eq}} s_{\text{eq}} dx = \int_0^L h_0 s_0 dx = \mathcal{S}_0. \quad (4.3d)$$

The existence of such equilibrium solutions depends on the effective salt capacity profile  $\bar{S}(x)$  and other parameters. For instance, with initial condition constraint  $\mathcal{S}_0 = 2$  and the form of  $\bar{S}$  given by (4.2) with varying width  $w$ , the equilibrium solutions to (1.1) with  $(m, n) = (3.5, 4.5)$  are calculated via a continuation method and are plotted in Fig. 5. Note that for smaller  $w$  in (4.2) the steady state  $h_{\text{eq}}$  has a positive lower bound, while the minimum of  $h_{\text{eq}}$  approaches zero at  $x = 1$  with  $w \sim 0.314$ . This result suggests that steady states for (1.1) with  $\mathcal{S}_0 = 2$  and  $(m, n) = (3.5, 4.5)$  do not exist for  $w > 0.314$  for  $\bar{S}$  given by (4.2). It is interesting that while  $\min h_{\text{eq}}$  is monotonically decreasing in terms of  $w$ , the profile of the equilibrium osmolarity  $s_{\text{eq}}$  changes dramatically and  $\max s_{\text{eq}}$  is not monotone in  $w$ , as is shown in Fig. 5 (right).

Fig. 6 depicts a typical simulation of the model (1.1) with the total mass of salt  $\mathcal{S}_0 = 2$ ,  $w = 0.2$  and  $(m, n) = (3.5, 4.5)$ , showing convergence of PDE solutions (dashed lines) to equilibrium solutions  $(h_{\text{eq}}, s_{\text{eq}})$  (solid lines) in the long time. Moreover, numerical observations for  $m > 1$  indicate that PDE solutions of (1.1) converge to the corresponding equilibrium which satisfies (4.3). If the equilibrium does not exist, we expect infinite-time non-uniform thinning with  $h \rightarrow 0$  at a critical point  $x_c$  as  $t \rightarrow \infty$ . With the width  $w = 0.3$ , a set of PDE simulations starting from identical initial data are plotted in Fig. 7 with  $h_{\min}$  decreasing in time. Three distinct regimes are developed in this case: for region (a) with  $0 \leq m \leq 1$  finite-time singularity develops similar to the case shown in Fig. 3; For region (c) with  $m \geq 3.5$  the PDE solution converges to an equilibrium solution  $(h_{\text{eq}}, s_{\text{eq}})$  similar to the dynamics in Fig. 6; While for region (b) with  $1 < m \leq 3$  the minimum film thickness approaches zero as  $t \rightarrow \infty$ . Specifically, in the neighborhood of  $x_c$  where  $h \rightarrow 0$ , the film thickness profile forms a nearly flat plateau with the corresponding  $s \ll \bar{S}$ . Therefore from (1.1a) the minimum film thickness is asymptotically determined by

$$\frac{d}{dt} h_{\min} \sim -\eta h_{\min}^m, \quad \text{where } \eta = \bar{S}(x_c),$$

which leads to an estimate of the rate of change of  $h_{\min}$  in time,

$$h_{\min}(t) \sim (c + \eta(m-1)t)^{-\frac{1}{m-1}}, \quad (4.4)$$

where  $c$  is a constant that depends on other system parameters and initial conditions. The comparison of the direct PDE simulations against the prediction  $h_{\min}(t) = O(t^{-\frac{1}{m-1}})$  as  $t \rightarrow \infty$  for regime (b) in Fig. 7 shows good agreement with this estimate in the final stage as  $h_{\min} \rightarrow 0$ . The estimate in (4.4) also suggests that infinite-time thinning cannot happen for  $m < 1$ .

The dynamics in Fig. 7 can be understood by looking at Fig. 8 where the minimum film thickness of the equilibrium  $h_{\text{eq}}$  is plotted

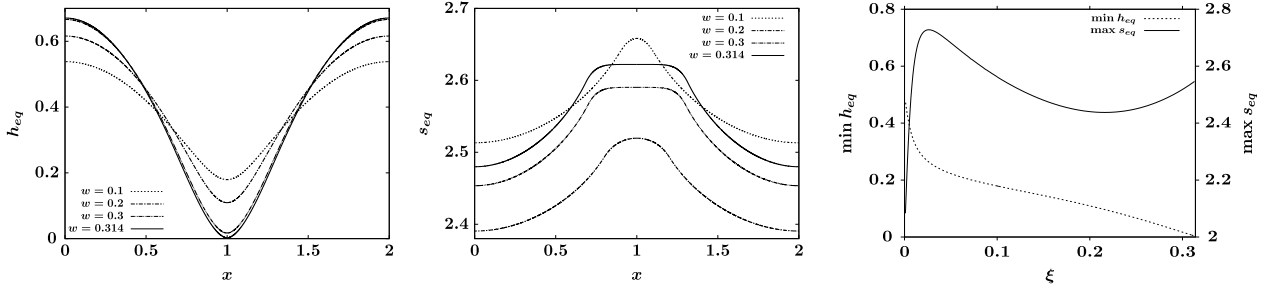


**Fig. 5.** Equilibrium solutions ( $h_{eq}, s_{eq}$ ) of (1.1) satisfying (4.3) with  $(m, n) = (3.5, 4.5)$ ,  $\bar{S}$  given by (4.2) with  $w = 0.1, \dots, 0.314$  and  $\int_0^L h_{eq} s_{eq} dx = 2$ . (Left)  $h_{eq}$  profiles; (middle)  $s_{eq}$  profiles; (right) plots of  $\min h_{eq}$  and  $\max s_{eq}$  vs. the width  $w$ .

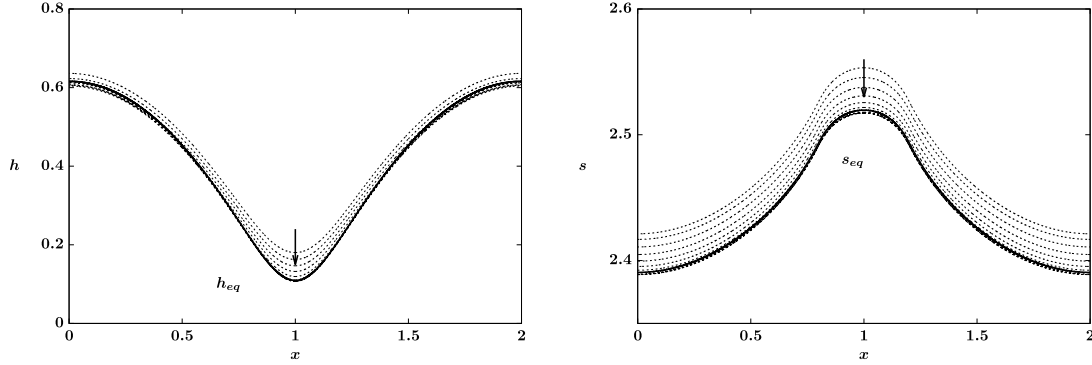


**Fig. 6.** Convergence of PDE solutions  $h$  and  $s$  (in dashed lines) to the equilibrium plotted in solid lines which satisfy the ODEs (4.3) with  $(m, n) = (3.5, 4.5)$  and  $\bar{S}$  from (4.2) with  $w = 0.2$ .

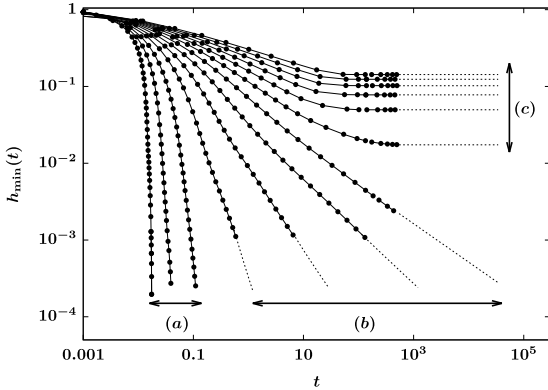


**Fig. 7.** Plots of minimum film thickness  $h_{min}$  with identical system parameters used in Fig. 4 and  $\bar{S}$  from (4.2) with  $w = 0.3$ . Region (a)  $m = 0, 0.5, 1$ ; Region (b)  $m = 1.5, 2, 2.5, 3$ ; Region (c)  $m = 3.5, 4, \dots, 6$ . Numerical results are represented by dotted lines, showing finite time singularity for region (a), infinite time thinning for region (b) following predictions from (4.4) plotted in dashed lines, and convergence of PDE solutions to steady states for region (c).

in terms of the width  $w$  in (4.2) and mobility coefficient  $m$ . It is shown in Fig. 8 that for  $0 < w < 0.1$ , the Eqs. (1.1) have an equilibrium ( $h_{eq}, s_{eq}$ ) for all positive  $m$ , while for  $w \geq 0.1$  there exists a critical  $m_c$  such that for  $m > m_c$  the equilibrium solution ( $h_{eq}, s_{eq}$ ) to the system (4.3) exists. Specifically, for  $w = 0.3$  in (4.2), results in Fig. 8 indicate that equilibrium solutions that satisfy the ODE system (4.3) only exist for  $m > m_c \approx 3.26$ . Therefore the threshold  $m = m_c$  divides the long-time behaviors of the PDE solutions into the two cases: infinite-time thinning with  $m < m_c$  and convergence to equilibrium with  $m > m_c$ .

## 5. Conclusions

In this work, the proof of global and local existence of solutions to the generalized tear film rupture model (1.1) with different

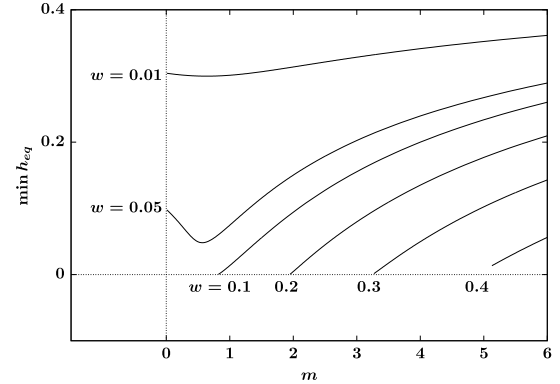


**Fig. 8.** Plots of the minimum film thickness of the steady states  $h_{eq}$  against system parameters  $m$  and  $n = m + 1$  with a set of  $w$  values, showing that for  $w > 0.1$  steady state solutions to (4.3) cease to exist when  $m$  is smaller than a critical value  $m_c$ . In particular, for  $w = 0.3$  the critical value of  $m$  is  $m_c = 3.26$ .

system parameters regimes has been carried out. More precisely, we have shown that with mobility exponents  $n = m + 1$  and  $3 \leq m \leq 4$  solutions to (1.1) exist globally, and local solutions to the model exist for the regime  $m \geq 0, n \geq 0$ .

The numerical results in Section 4 support the conclusion of the regularity and existence of solutions in Section 3. Specifically, the long time behavior of the PDE solutions to (1.1) with a family of  $\bar{S}$  profiles (4.2) is investigated. For the case  $n = m + 1$  and  $3 \leq m \leq 4$ , if an equilibrium solution ( $h_{eq}, s_{eq}$ ) can be established in the PDE system associated with a specified total mass of salt  $\delta$ , the PDE solutions approach to the equilibrium solution in the long time. Otherwise, without the attraction of the equilibrium, infinite-time non-uniform thinning in  $h$  is expected to happen. While with mobility exponents  $(m, n)$  outside the above region, for instance, with  $(m, n) = (0, 3)$  in the physical model (2.10), we numerically capture the formation of finite time singularity in both  $h$  and  $s$  driven by the non-conservative terms in the model.

Several interesting questions regarding the PDE (1.1) remain to be solved. First, in this paper we have restricted our attention to the scenario where  $n = m + 1$  and  $3 \leq m \leq 4$  for the proof of global existence of solutions. However, as is suggested by the set of simulations shown in Figs. 4 and 7, the parameter range for the existence of solutions can possibly be extended to larger regions. Inspired by the convergence of PDE solutions to equilibrium solutions in some of the numerical simulations, we are also interested to study whether the equilibrium solutions to (1.1) are all global attractors. More specifically, we may ask: does any solution converge to the equilibrium solutions, or how the existence of those equilibrium solutions depend on  $\tilde{S}$ , and system parameters  $(m, n)$ .

## Acknowledgments

This work was supported by the National Science Foundation under Grant No. DMS-1514826 and KI-Net RNMS11-07444.

## References

- [1] C.-C. Peng, C. Cerretani, R.J. Braun, C.J. Radke, Evaporation-driven instability of the precorneal tear film, *Adv. Colloid Interface Sci.* 206 (2014) 250–264.
- [2] D. Gilbarg, N.S. Trudinger, *Elliptic Partial Differential Equations of Second Order*, Springer, 2015.
- [3] R.J. Braun, Dynamics of the tear film, *Annu. Rev. Fluid Mech.* 44 (2012) 267–297.
- [4] F.J. Holly, Formation and rupture of the tear film, *Exp. Eye Res.* 15 (5) (1973) 515–525.
- [5] S.P. Lin, H. Brenner, Marangoni convection in a tear film, *J. Colloid Interface Sci.* 85 (1) (1982) 59–65.
- [6] A. Sharma, E. Ruckenstein, Mechanism of tear film rupture and its implications for contact lens tolerance, *Optom. Vis. Sci.* 62 (4) (1985) 246–253.
- [7] P.E. King-Smith, J.J. Nichols, K.K. Nichols, B.A. Fink, R.J. Braun, Contributions of evaporation and other mechanisms to tear film thinning and break-up, *Optom. Vis. Sci.* 85 (8) (2008) 623–630.
- [8] E. King-Smith, B. Fink, R. Hill, K. Koelling, J. Tiffany, The thickness of the tear film, *Curr. Eye Res.* 29 (4–5) (2004) 357–368.
- [9] R.E. Berger, S. Corrsin, A surface tension gradient mechanism for driving the pre-corneal tear film after a blink, *J. Biomech.* 7 (3) (1974) 225–238.
- [10] R.V. Craster, O.K. Matar, Dynamics and stability of thin liquid films, *Rev. Mod. Phys.* 81 (3) (2009) 1131.
- [11] S.G. Yiantsios, B.G. Higgins, A mechanism of Marangoni instability in evaporating thin liquid films due to soluble surfactant, *Phys. Fluids* 22 (2) (2010) 022102.
- [12] E.R. Peterson, M. Shearer, Simulation of spreading surfactant on a thin liquid film, *Appl. Math. Comput.* 218 (9) (2012) 5157–5167.
- [13] B.P. Cook, A.L. Bertozzi, A.E. Hosoi, Shock solutions for particle-laden thin films, *SIAM J. Appl. Math.* 68 (3) (2008) 760–783.
- [14] S.D. Howison, J.A. Moriarty, J.R. Ockendon, E.L. Terrill, S.K. Wilson, A mathematical model for drying paint layers, *J. Engrg. Math.* 32 (4) (1997) 377–394.
- [15] P.L. Evans, L.W. Schwartz, R.V. Roy, A mathematical model for crater defect formation in a drying paint layer, *J. Colloid Interface Sci.* 227 (1) (2000) 191–205.
- [16] L. Li, R.J. Braun, A model for the human tear film with heating from within the eye, *Phys. Fluids* 24 (6) (2012) 062103.
- [17] J.I. Siddique, R.J. Braun, Tear film dynamics with evaporation, osmolarity and surfactant transport, *Appl. Math. Model.* 39 (1) (2015) 255–269.
- [18] R.J. Braun, P.E. King-Smith, J.J. Nichols, P. Ramamoorthy, On computational models for tear film and osmolarity dynamics, in: 6th International Conference on the Tear Film and Ocular Surface: Basic Science and Clinical Relevance, 2010.
- [19] K.N. Winter, D.M. Anderson, R.J. Braun, A model for wetting and evaporation of a post-blink precorneal tear film, *Math. Med. Biol.* 27 (2010) 211–225.
- [20] J.P. Burelbach, S.G. Bankoff, S.H. Davis, Nonlinear stability of evaporating/condensing liquid films, *J. Fluid Mech.* 195 (1988) 463–494.
- [21] V.S. Ajaev, Spreading of thin volatile liquid droplets on uniformly heated surfaces, *J. Fluid Mech.* 528 (2005) 279–296.
- [22] V.S. Ajaev, Evolution of dry patches in evaporating liquid films, *Phys. Rev. E* 72 (3) (2005) 031605.
- [23] S. Mishima, D.M. Maurice, The oily layer of the tear film and evaporation from the corneal surface, *Exp. Eye Res.* 1 (1) (1961) 39–45.
- [24] A.J. Majda, A.L. Bertozzi, *Vorticity and Incompressible Flow*, Vol. 27, Cambridge University Press, 2002.
- [25] O.E. Jensen, J.B. Grotberg, Insoluble surfactant spreading on a thin viscous film: shock evolution and film rupture, *J. Fluid Mech.* 240 (1992) 259–288.
- [26] M. Renardy, A singularly perturbed problem related to surfactant spreading on thin films, *Nonlinear Anal. TMA* 27 (3) (1996) 287–296.
- [27] H.B. Keller, A new difference scheme for parabolic problems, in: *Numerical Solution of Partial Differential Equations*, Vol. II, SYNSPADE 1970, 1971, pp. 327–350.
- [28] H.D. Ceniceros, T.Y. Hou, An efficient dynamically adaptive mesh for potentially singular solutions, *J. Comput. Phys.* 172 (2) (2001) 609–639.